






RESEARCH ARTICLE | OCTOBER 31 2023

## Terahertz study of ambipolar transport in the semiconducting polymer poly-diketopyrrolopyrrole-terthiophene (PDPP3T)

P. Riederer ; C. Eckel ; R. T. Weitz ; R. Kersting  



*Appl. Phys. Lett.* 123, 182104 (2023)

<https://doi.org/10.1063/5.0166449>

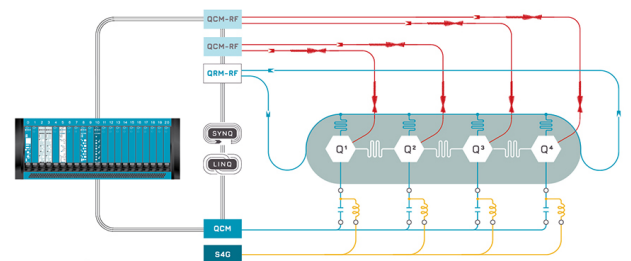


CrossMark



Integrates all Instrumentation + Software for Control and Readout of

**Superconducting Qubits**  
**NV-Centers**  
**Spin Qubits**



Superconducting Qubit Setup

[find out more >](#)

# Terahertz study of ambipolar transport in the semiconducting polymer poly-diketopyrrolopyrrole-terthiophene (PDPP3T)

Cite as: Appl. Phys. Lett. **123**, 182104 (2023); doi: [10.1063/5.0166449](https://doi.org/10.1063/5.0166449)

Submitted: 5 July 2023 · Accepted: 13 October 2023 ·

Published Online: 31 October 2023



View Online



Export Citation



CrossMark

P. Riederer,<sup>1</sup>  C. Eckel,<sup>2</sup>  R. T. Weitz,<sup>2,3</sup>  and R. Kersting<sup>1,a)</sup> 

## AFFILIATIONS

<sup>1</sup>Photonics and Optoelectronics Group, Faculty of Physics and Center for NanoScience (CeNS), Ludwig-Maximilians-Universität, Königinstr. 10, 80539 München, Germany

<sup>2</sup>1st Institute of Physics, Faculty of Physics, Georg-August-University, Göttingen, Germany

<sup>3</sup>International Center for Advanced Studies of Energy Conversion (ICASEC), University of Göttingen, Göttingen, Germany

<sup>a)</sup> Author to whom correspondence should be addressed: [roland.kersting@lmu.de](mailto:roland.kersting@lmu.de)

## ABSTRACT

Terahertz electromodulation spectroscopy is used to investigate charge transport in the semiconducting polymer poly-diketopyrrolopyrrole-terthiophene (PDPP3T). Both electrons and holes show band transport with a preferential conduction along the polymer chain. In devices with oriented thin-films, mobilities of 2.0 and 12.8 cm<sup>2</sup>/V s are measured for electrons and holes, respectively. Temperature-resolved and long-time measurements suggest that only a fraction of the injected charge carriers participate in band transport. Carrier trapping into localized states is identified as the major factor that limits the overall mobilities. According to the Ioffe–Regel criterion, the material's inherent mobilities are expected to significantly exceed the observed values.

© 2023 Author(s). All article content, except where otherwise noted, is licensed under a Creative Commons Attribution (CC BY) license (<http://creativecommons.org/licenses/by/4.0/>). <https://doi.org/10.1063/5.0166449>

The realization of n-channel conduction in organic field-effect devices is challenging partially because of the energy mismatch between the material's LUMO level and the Fermi energy of the injection metal.<sup>1</sup> Donor–acceptor polymers offer the opportunity to lower such injection barriers.<sup>2</sup> Alternating electron-rich and electron-deficient repeat units along the  $\pi$ -conjugated polymer backbone reduce the bandgap and bring the LUMO states within reach.<sup>3,4</sup> Although this supports charge carrier injection, the subsequent charge transport through the polymer is a complex interplay of intrinsic and extrinsic mechanisms.<sup>5</sup> Among the intrinsic transport processes are the fast band transport along the polymer backbone and the considerably slower transfer in perpendicular directions.<sup>6,7</sup> Extrinsic factors that hinder charge transport in polycrystalline thin-films are, for instance, the transfer across grain boundaries and the localization of charge carriers at defects. In light of this complexity, it appears reasonable to start with investigating the intrinsic properties of charge transport in semiconducting polymers.<sup>5,7</sup>

In this paper, we report terahertz (THz) experiments on poly-diketopyrrolopyrrole-terthiophene (PDPP3T) that provide insight into the material's intrinsic transport properties. An anisotropy of

conduction is observed in thin-films with partially aligned polymers. For transport along the chains, mobilities of  $\mu_e = 2.0$  cm<sup>2</sup>/V s and  $\mu_h = 12.8$  cm<sup>2</sup>/V s are derived for electrons and holes, respectively. The analysis indicates that these values should be understood as lower mobility limits, while the actual mobilities for transport along the chains significantly exceed these values.

The donor–acceptor polymer PDPP3T comprises 1,4-diketopyrrolo-(3,4-c)-pyrrole (DPP) groups with a terthiophene group between the DPP pairs. Figure 1(a) shows the molecular structure of the polymer used in this study. Alkyl side groups are often used to achieve dense molecular packaging, increase solubility, and enhance crystallinity.<sup>9,10</sup> For PDPP3T, a bandgap of  $E_g \approx 1.3$  eV has been reported.<sup>9</sup> In PDPP3T derivatives, hole mobilities of up to 10 cm<sup>2</sup>/V s have been observed on thin-film field-effect transistors (FETs),<sup>10–12</sup> and electron mobilities of up to 4.3 cm<sup>2</sup>/V s have been reported.<sup>10</sup> Furthermore, PDPP3T has shown to be able to carry large current densities above 1 MA/cm<sup>2</sup>.<sup>13,14</sup>

Terahertz spectroscopy is an ideal tool for investigating intrinsic transport properties because it exclusively probes the band transport of delocalized charge carriers. The resulting Drude transport usually shows mobilities that exceed 1 cm<sup>2</sup>/V s. The technique is insensitive to

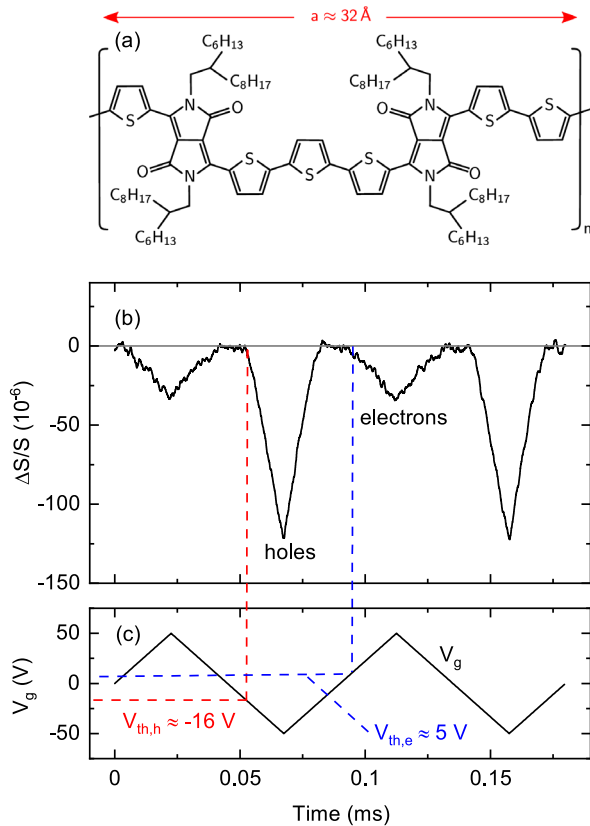


**FIG. 1.** (a) Unit cell of PDPP3T, which comprises two monomers, according to Ref. 8. Dependence of the THz transmission on charge injection, with (b) relative differential THz transmission and (c) applied gate voltage. The dashed lines indicate the threshold voltages  $V_{th,h}$  and  $V_{th,e}$  for holes and electrons, respectively.

low mobility transport due to hopping between localized states.<sup>15</sup> Previous THz studies on organic semiconductors have investigated the response of photoexcited charge carriers to the THz field.<sup>16–19</sup> However, in such experiments, both the photogenerated holes and the electrons interact with the transmitted THz radiation, and discerning their individual contributions to transport is challenging. In this study, to separate electron and hole transport, we use THz electromodulation spectroscopy,<sup>15,20,21</sup> where charge carriers are electronically injected into the semiconducting polymer.

Thin-film PDPP3T devices are fabricated on substrates of polyethylene naphthalate. The device architecture is shown in Fig. S1(a) of the supplementary material. A 6 nm thick chromium layer serves as gate contact, and a 300 nm thick layer of parylene N is the gate insulator. The PDPP3T has a molar mass of  $41 \times 10^3$  Da and is deposited by blade coating a solution of 5 mg/ml in meta-dichlorobenzene (MDCB), which leads to a film thickness of approximately 60 nm. A description of the deposition process can be found in section I of the supplementary material. Depending on the process parameters, thin-films with both aligned and unaligned polymers can be fabricated.<sup>22</sup> Injection contacts are fabricated on top of the PDPP3T by physical vapor deposition of 3 nm molybdenum oxide ( $\text{MoO}_x$ ), followed by 6 nm chromium (Cr). Details of

the fabrication process can be found in the supplementary material and in Refs. 13 and 15.

Terahertz pulses with a bandwidth of 2.5 THz are transmitted through the thin-film devices. The THz pulses are linearly polarized, which allows to study how charge carrier transport depends on the orientation of the polymer chains. In all experiments, the transmission is recorded at the temporal peak of the THz pulse (Fig. S2). As shown in Fig. 1, the transmission depends on the applied voltage  $V_g$  between the chromium gate and the injection layer. At negative gate voltages, holes are injected from the  $\text{MoO}_x/\text{Cr}$  injection layer into the PDPP3T, where they accumulate at the interface with the parylene insulator. The free-carrier response of the holes reduces the transmission of radiation through the device.<sup>15,20</sup> The same is observed when electrons are injected at positive gate voltages. For both, holes and electrons, the relative differential transmission  $\Delta S/S$  follows almost linearly  $V_g$ . Holes are injected after a threshold of  $V_{th,h} \approx -16$  V is reached, while the threshold for electron injection is  $V_{th,e} \approx 5$  V.

The carriers' sheet conductivity  $\sigma_{2D}$  and their mobility  $\mu$  are related to the observed relative differential transmission  $\Delta S/S$  by the equivalent of Tinkham's formula for electric field transmission,<sup>23,24</sup>

$$\sigma_{2D} = e\mu n_{2D,mob} = \frac{-\Delta S}{S} \cdot \frac{2\sqrt{\epsilon_b}}{Z_0}, \quad (1)$$

where  $\epsilon_b = 2.8$  is assumed for the relative background permittivity of the semiconductor,  $Z_0 = 376.7 \Omega$  is the impedance of free space, and  $n_{2D,mob}$  stands for the sheet density of the mobile carriers. Multiple reflections of THz radiation within the device do not contribute to the conductivities obtained by Eq. (1) because relative differential measurements by electro-modulation cancel out the static properties of the device architecture.

According to Eq. (1), the carriers' sheet conductance can be obtained with high reliability because  $\Delta S/S$  is a relative differential transmission signal. The determination of the charge carriers' mobility  $\mu$ , however, depends on the precise knowledge of the density of mobile charges  $n_{2D,mob}$  that participate in band transport. Because of trapping,  $n_{2D,mob}$  is smaller than the injected charge carrier density  $n_{2D,inj}$ , which can be deduced from the device's unit capacitance  $\bar{C}$  and the applied voltage  $V_g$ . The device used in Fig. 1 has a unit capacitance  $\bar{C} = 6.8$  nF/cm<sup>2</sup>, which, at the maximum of the applied gate voltage  $V_g = \pm 50$  V, leads to a density of injected carriers  $n_{inj} = 2.1 \times 10^{12}$  cm<sup>-2</sup>. Assuming that all injected charge carriers are mobile, the evaluation according to Eq. (1) provides electron and hole mobilities of  $\mu_e = 0.8$  cm<sup>2</sup>/V s and  $\mu_h = 3.3$  cm<sup>2</sup>/V s, respectively. Similar mobilities have been observed on PDPP3T FETs.<sup>10–12</sup>

The data presented in Fig. 1 are recorded on an unoriented nanocrystalline thin-film. The atomic force micrographs (AFMs) of this particular film show neither elongated nanocrystals nor a preferred orientation of the sample's topography (Fig. S3). The question we want to address is how mesoscopic order and trapping affect mobility. As shown in Fig. 2, considerably higher mobilities are deduced on films that comprise elongated nanocrystals, which are oriented by blade coating. On these structures, electron and hole mobilities reach  $\mu_e = 2.0$  cm<sup>2</sup>/V s and  $\mu_h = 12.8$  cm<sup>2</sup>/V s, respectively. The observed threshold voltages are not considered in the deduction of these values. Considering them leads to  $\mu_e = 2.2$  cm<sup>2</sup>/V s and  $\mu_h = 18.8$  cm<sup>2</sup>/V s, for the fractions of those carriers that are mobile. The density of mobile carriers, however, depends on time as shown in Fig. 5, and, thus, we refrain from using these values.

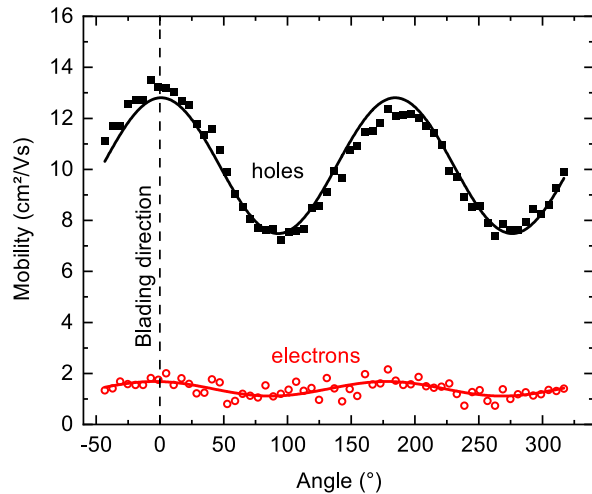


**FIG. 2.** Carrier mobilities in dependence of the angle between blading direction and polarization of the THz beam. The dashed line indicates the blading direction. The deduced mobilities of electrons and holes are shown by red circles and black squares, respectively. The solid lines show sinusoidal fits to the experimental data.

More striking is the angular dependence of the mobility when the device is rotated around the propagation direction of the THz beam. Mobility maxima are observed when the electrical field of the THz pulses is oriented parallel to the blading direction. The solid lines are sinusoidal fits to the electron and hole mobilities. Both fits show the same phase. Studies of FETs fabricated on oriented thin-films have found similar orientation dependencies, as summarized in Ref. 25. Nanoscale charge transport experiments of PDPP3T fibers have also revealed sizable hole and electron mobilities consistent with our THz measurements.<sup>26</sup> Probing photoconductivity with THz radiation has revealed a polarization anisotropy and has been interpreted by preferential charge conduction along the polymer backbone.<sup>19</sup>

The observed angular dependence of the THz signal agrees with the topological properties of the PDPP3T film. The AFM data presented in Fig. 3(a) show crystallites with a length of approximately 160 nm and a width of 40 nm. The alignment of the crystallites becomes visible in the two-dimensional Fourier transform. In the first and third quadrants, amplitudes at small wave vectors are mostly observed, which indicates large-wavelength oscillations of the thin-film's height. Thus, the crystals are primarily aligned from the lower left corner of the AFM to the top right corner. Also shown in Fig. 3(b) is an ellipse, which indicates the polarization anisotropy shown in Fig. 2. The lengths of the ellipse's semiaxes are proportional to the minimum and maximum values of the hole mobilities. The orientation of the ellipse reproduces the distribution of the Fourier transform's amplitudes, which suggests that transport along the polymer chains is faster than transport perpendicular to the chain direction—that is, charge transfer from one molecule to a neighboring molecule. This holds true for both electron and hole transports because both exhibit the same angular dependence, as shown in Fig. 2. The thin-film's crystals, however, are only partially oriented. Thus, the minima of the mobility data shown in Fig. 2 should not be understood as the mobility for intermolecular carrier transport.

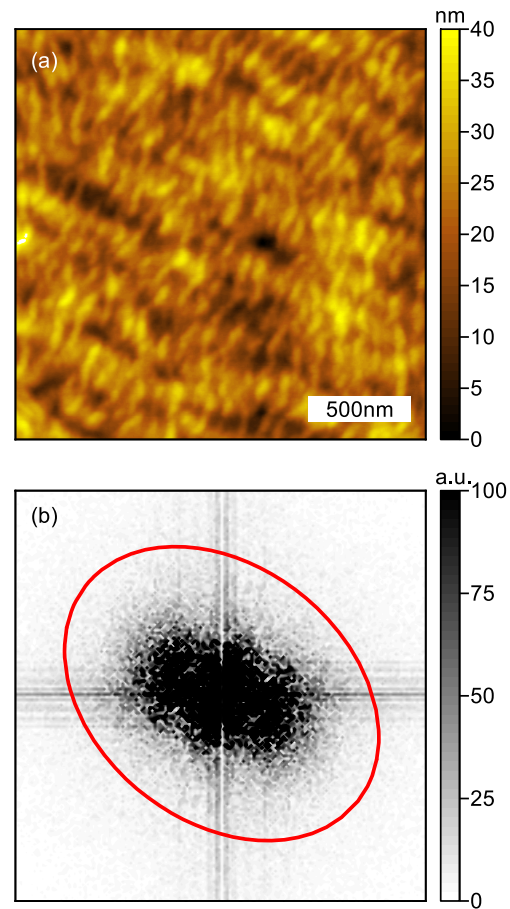


**FIG. 3.** (a) Atomic force micrograph of the PDPP3T layer of the device, on which the data shown in Fig. 2 are recorded. (b) Excerpt of the two-dimensional Fourier transform of the AFM data. The black dots show the amplitude of the FFT data. The red line illustrates the angular dependence of the hole mobility data shown in Fig. 2.

Are  $\mu_e = 2.0 \text{ cm}^2/\text{V s}$  and  $\mu_h = 12.8 \text{ cm}^2/\text{V s}$  the charge carriers' intrinsic mobilities? An insight is gained by looking at the charge carriers' thermal mean free path, which is for one-dimensional motion, given by

$$\ell_{th} = \frac{\mu}{e} \sqrt{k_B T m^*}. \quad (2)$$

For temperature,  $T = 300 \text{ K}$  is used, and for the effective carrier mass,  $m^* = m_e$  is assumed. The aforementioned mobilities provide  $\ell_{th,e} \approx 0.8 \text{ \AA}$  and  $\ell_{th,h} \approx 4.9 \text{ \AA}$ . However, the length of the unit cell along the polymer's backbone is  $a \approx 32 \text{ \AA}$ .<sup>8</sup> Both the electron and hole mean free paths are significantly smaller than the unit cell and even smaller than the monomer. This contradicts the Ioffe-Regel criterion,<sup>27,28</sup> according to which Bloch waves can exist only if  $\ell_{th} \gg a$ . The criterion is a prerequisite for band transport. For  $\ell_{th} < a$ , charge carriers are localized and can proceed only by hopping transport, which usually leads to  $\mu < 1 \text{ cm}^2/\text{V s}$ . However, such slow transport processes cannot be detected using THz spectroscopy.<sup>15</sup> Moreover, the

observed mobilities of up to  $12.8 \text{ cm}^2/\text{Vs}$  contradict hopping transport.

The aforementioned contradictions are resolved, if only a fraction of the injected charge carriers are mobile and interact with the transmitted THz radiation. According to Eq. (1), values of  $n_{2D,mob} \ll n_{2D,inj}$  lift the mobility  $\mu$  for the same transmission change  $\Delta S/S$ . With an increase in  $\mu$ , the thermal mean free path  $\ell_{th}$  also increases, and the Ioffe–Regel criterion can be fulfilled. Although this consideration does not allow us to deduce the actual mobilities of mobile electrons and holes, it shows that only a minor fraction of the injected charge carriers are mobile and participate in Bloch transport. Consequently, carriers that propagate along the polymer chain are expected to have mobilities that by far exceed  $\mu_e = 2.2 \text{ cm}^2/\text{Vs}$  and  $\mu_h = 12.8 \text{ cm}^2/\text{Vs}$ , which are deduced by assuming  $n_{2D,mob} = n_{2D,inj}$ .

Temperature-resolved experiments support this notion. As shown in Fig. 4, the electron and hole mobilities rapidly diminish with decreasing temperature. The observed decrease fits neither the temperature dependence of Eq. (2) nor other processes, such as phonon scattering, which should show  $\mu \sim T^{-3/2}$ . We propose that the decrease is due to mobile carriers being trapped in localized states, from which they cannot be reemitted into band states, especially at low temperatures.

The long-time dependence of the THz transmission also indicates that a significant fraction of the injected carriers are trapped. Figure 5(a) shows the gate voltage applied to record how hole transport evolves on time-scales up to 200 s. To measure electron transport, an equivalent signal with opposite polarity is applied. The THz signal is recorded only during the period of modulation after  $t > 0$  s. The inset shows the 2 Hz modulation, which provides the relative differential signal  $\Delta S/S$  due to the THz response of the mobile carriers. The purpose of the long-time pulses at  $t < 0$  s is to establish a well-defined state within the device before the measurement starts. For instance, the pulse with  $V_g = +50$  V between  $t = -60$  s and  $t = 0$  s depletes the structure from holes immobilized in traps.

Figure 5(b) shows how the THz signal evolves after  $t = 0$  s. Every data point is obtained by averaging  $\Delta S/S$  over a time interval of

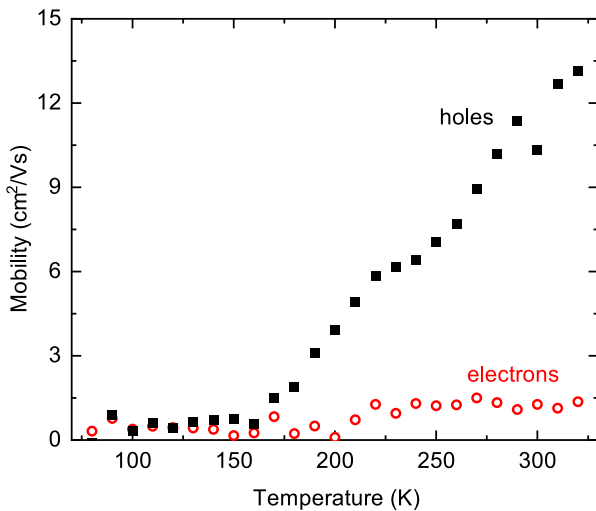


FIG. 4. Temperature dependence of electron and hole mobilities. The mobilities are deduced by assuming that all injected charge carriers participate in band transport.

$\Delta t \approx 8$  s before recording data for the next point. Shown is the averaged signal  $\Delta S(t)/S(t)$  after 120 repetitions over the time interval from  $t = 0$  s to  $t = 200$  s. For holes, the average of  $\Delta S(t)/S(t)$  decreases with a time constant of 50 s. The temporal dependence of the electron signal is weak, and we refrain from interpreting it. The dynamics of the hole signal shows that part of the injected holes is trapped and cannot be removed from the device during the modulation cycle, which has a maximum voltage of  $V_g = -2$  V. A significant number of holes may be already trapped during the accumulation time, which is required for recording the first data point. The trapped holes build up a polarization, which counteracts the injection of further charges during the next modulation cycle. With increasing time, progressively fewer mobile holes are injected and contribute to the THz signal. With the following scan, the polarization of the device is reset by the positive prepulse at  $-60 \text{ s} \leq t \leq 0$  s, which withdraws the trapped charges.

Figure 6 summarizes the proposed dynamics. With the application of  $V_g < 0$ , holes are injected from the  $\text{MoO}_x$  contact into the PDPP3T and drift toward the interface with the insulator (a). The charge carriers accumulate at the interface (b). The thickness of this layer results from the interplay between Poisson’s equation and Fermi–Dirac statistics and has a thickness of a few angstroms.<sup>29</sup> In the region between this layer and the injection contacts, the applied field is screened by the accumulated charges. The holes within the accumulation region are trapped in defects (c). Their states are deep within the bandgap, which prevents

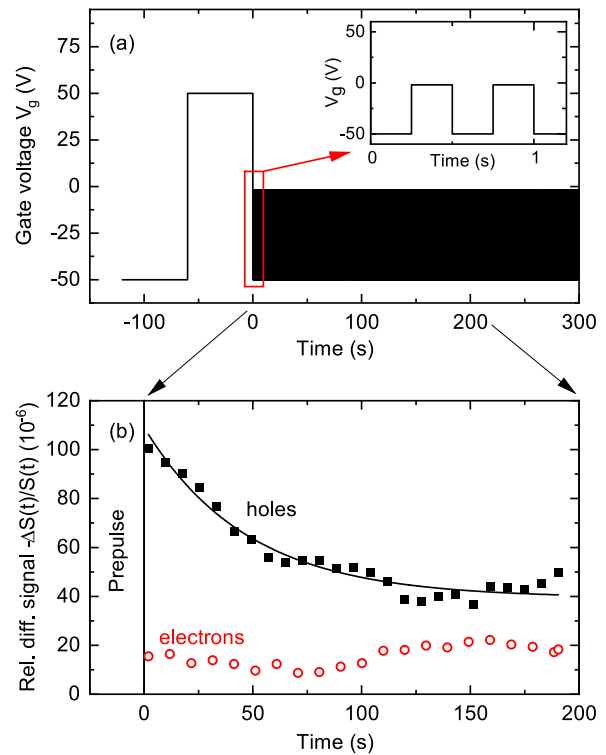
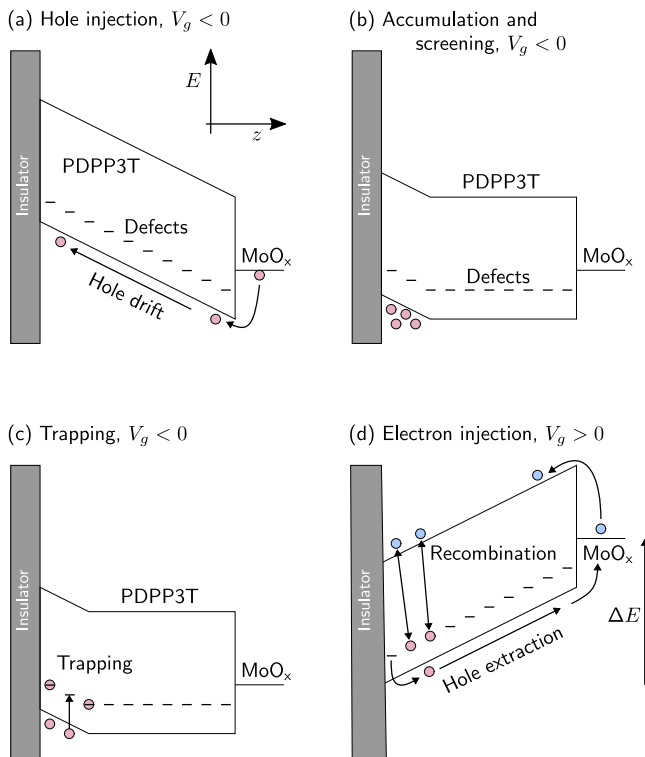


FIG. 5. Change of the THz transmission signal over time. (a) Applied pulse sequence of the gate voltage. The inset shows two of the modulation cycles. (b) Time dependence of the averaged signal  $-\Delta S(t)/S(t)$  after the two initializing pulses. The dynamics of electrons and holes are indicated by red circles and black squares, respectively. The solid line serves as a guide for the eye.



**FIG. 6.** Model of the band structure  $E(z)$  within the device. (a) Holes are injected from the  $\text{MoO}_x$  layer, (b) accumulate at the interface with the semiconductor, (c) and are trapped in defect states. (d) The application of  $V_g > 0$  depletes the traps from holes. For clarity, the band structure in (d) is shifted by  $\Delta E$ .

them from being reemitted into the valence band, and the density of mobile holes is reduced. The trapped states cause a permanent polarization between the accumulation layer and the gate contact. Because the defect states are within the bandgap, the application of  $V_g = 0$  V would not suffice to empty the traps and transfer the holes back into the injection contact. During a modulation cycle between  $V_g = -50$  V and  $V_g = 0$  V, these carriers remain trapped, and their polarization prevents the injection of mobile holes. Only a gate bias of  $V_g > 0$  can remove the trapped holes (d). This may occur via transport within the valence band. Alternatively, the trapped holes may recombine with electrons that are injected at  $V_g > 0$ . Many works have discussed similar mechanisms as the origins of voltage thresholds and hysteresis of FETs of molecular semiconductors—for instance, Refs. 30 and 31.

The model that only a minor fraction of the injected charges participate in band transport agrees with four main results of this work: (i) According to the Ioffe–Regel criterion, the carriers' thermal mean free path  $\ell_{th}$  must exceed the size of the unit cell. This is possible only if the observed conductance  $\sigma_{2D}$  results from carriers with high mobility, although their density may be lower than that of the injected carriers. (ii) The temperature dependence of the hole mobility suggests that even at room temperature, a significant fraction of the injected holes are localized. (iii) The observed conductance of holes decreases with a time constant of 50 s. The original conductance can be reached again only after applying an oppositely poled gate voltage. (iv) For holes, an injection threshold  $V_{th,h} = -16$  V is observed, which

is in accordance with a built-in polarization that counteracts hole injection.

In summary, THz electromodulation spectroscopy provides insights into carrier transport in PDPPP3T thin-film devices. Both hole transport and electron transport are observed. Structures with unaligned PDPPP3T crystallites have smaller conductance than devices with aligned crystals. Polarization-dependent measurements show that the conduction is enhanced along the backbone of the polymer. On oriented thin-films, mobilities of 2.0 and 12.8  $\text{cm}^2/\text{Vs}$  are observed for electrons and holes, respectively. However, the associated thermal mean free paths are significantly smaller than the unit cells along the polymer backbone. This violates the Ioffe–Regel criterion and indicates that only a fraction of the injected carriers participate in band transport. These carriers should have a material-inherent mobility that significantly exceeds the aforementioned values. This is confirmed by temperature-resolved studies and long-time measurements. Altogether, the results indicate that disorder in P3PP3T thin-films causes trapping and decreased overall mobility. Reducing defects appears to be of utmost importance for realizing high-mobility polymeric semiconductors.

See the supplementary material for details on the fabrication of PDPPP3T thin-films, device architecture, terahertz electromodulation spectroscopy, the used atomic force microscope, and results on unaligned films.

This research was funded by German Research Foundation (Deutsche Forschungsgemeinschaft), Grant No. KE 516/11-1. R.T.W. acknowledges funding from the SFB 1073 “Atomic scale control of energy conversion.” The authors thank K. Lechermann for his technical help.

## AUTHOR DECLARATIONS

### Conflict of Interest

The authors have no conflicts to disclose.

## Author Contributions

**Philipp Riederer:** Data curation (equal); Formal analysis (equal); Visualization (equal); Writing – original draft (equal); Writing – review & editing (equal). **Christian Eckel:** Data curation (equal); Formal analysis (supporting); Resources (lead); Writing – original draft (supporting); Writing – review & editing (equal). **R. Thomas Weitz:** Conceptualization (equal); Project administration (equal); Resources (supporting); Supervision (equal); Writing – review & editing (equal). **Roland Kersting:** Conceptualization (lead); Formal analysis (equal); Funding acquisition (equal); Project administration (equal); Supervision (equal); Visualization (equal); Writing – original draft (lead); Writing – review & editing (equal).

## DATA AVAILABILITY

The data that support the findings of this study are available from the corresponding author upon reasonable request.

## REFERENCES

- J. Zaumseil and H. Sirringhaus, “Electron and ambipolar transport in organic field-effect transistors,” *Chem. Rev.* **107**, 1296 (2007).

- <sup>2</sup>K. Müllen and W. Pisula, "Donor-acceptor polymers," *J. Am. Chem. Soc.* **137**, 9503 (2015).
- <sup>3</sup>E. E. Havinga, W. ten Hoeve, and H. Wynberg, "Alternate donor-acceptor small-band-gap semiconducting polymers; Polysquaraines and polycrocenines," *Synth. Met.* **55**, 299 (1993).
- <sup>4</sup>A. Ajayaghosh, "Donor-acceptor type low band gap polymers: Polysquaraines and related systems," *Chem. Soc. Rev.* **32**, 181 (2003).
- <sup>5</sup>B. B.-Y. Hsu, C.-M. Cheng, C. Luo, S. N. Patel, C. Zhong, H. Sun, J. Sherman, B. H. Lee, L. Ying, M. Wang, G. Bazan, M. Chabiniyc, J.-L. Bredas, and A. Heeger, "The density of states and the transport effective mass in a highly oriented semiconducting polymer: Electronic delocalization in 1D," *Adv. Mater.* **27**, 7759 (2015).
- <sup>6</sup>H. N. Tsao and K. Müllen, "Improving polymer transistor performance via morphology control," *Chem. Soc. Rev.* **39**, 2372 (2010).
- <sup>7</sup>J. Lenz and R. T. Weitz, "Charge transport in semiconducting polymers at the nanoscale," *APL Mater.* **9**, 110902 (2021).
- <sup>8</sup>A. Alesadi, F. Fatima, W. Xia, and D. Kilin, "First-principles study on the electronic properties of PDPP-based conjugated polymer via density functional theory," *J. Phys. Chem. B* **125**, 8953 (2021).
- <sup>9</sup>J. C. Bijleveld, A. P. Zoombelt, S. G. J. Mathijssen, M. M. Wienk, M. Turbiez, D. M. de Leeuw, and R. A. J. Janssen, "Poly(diketopyrrolopyrrole-terthiophene) for ambipolar logic and photovoltaics," *J. Am. Chem. Soc.* **131**, 16616 (2009).
- <sup>10</sup>J. Lee, A.-R. Han, H. Yu, T. J. Shin, C. Yang, and J. H. Oh, "Boosting the ambipolar performance of solution-processable polymer semiconductors via hybrid side-chain engineering," *J. Am. Chem. Soc.* **135**, 9540 (2013).
- <sup>11</sup>I. Kang, H.-J. Yun, D. S. Chung, S.-K. Kwon, and Y.-H. Kim, "Record high hole mobility in polymer semiconductors via side-chain engineering," *J. Am. Chem. Soc.* **135**, 14896 (2013).
- <sup>12</sup>S.-F. Yang, Z.-T. Liu, Z.-X. Cai, M. J. Dyson, N. Stingelin, W. Chen, H.-J. Ju, G.-X. Zhang, and D.-Q. Zhang, "Diketopyrrolopyrrole-based conjugated polymer entailing triethylene glycols as side chains with high thin-film charge mobility without post-treatments," *Adv. Sci.* **4**, 1700048 (2017).
- <sup>13</sup>J. Lenz, F. Del Giudice, F. R. Geisenhof, F. Winterer, and R. T. Weitz, "Vertical, electrolyte-gated organic transistors show continuous operation in the MA cm<sup>-2</sup> regime and artificial synaptic behaviour," *Nat. Nanotechnol.* **14**, 579 (2019).
- <sup>14</sup>J. Lenz, A. M. Seiler, F. R. Geisenhof, F. Winterer, K. Watanabe, T. Taniguchi, and R. T. Weitz, "High-performance vertical organic transistors of sub-5 nm channel length," *Nano Lett.* **21**, 4430 (2021).
- <sup>15</sup>P. Riederer and R. Kersting, "Terahertz electromodulation spectroscopy for characterizing electronic transport in organic semiconductor thin films," *J. Infrared Millimeter, Terahertz Waves* **44**, 1 (2023).
- <sup>16</sup>E. Hendry, M. Koeberg, J. M. Schins, H. K. Nienhuys, V. Sundstrom, L. D. A. Siebbeles, and M. Bonn, "Interchain effects in the ultrafast photophysics of a semiconducting polymer: THz time-domain spectroscopy of thin films and isolated chains in solution," *Phys. Rev. B* **71**, 125201 (2005).
- <sup>17</sup>P. Parkinson, J. Lloyd-Huges, M. B. Johnston, and L. M. Herz, "Efficient generation of charges via below-gap photoexcitation of polymer-fullerene blend films investigated by terahertz spectroscopy," *Phys. Rev. B* **78**, 115321 (2008).
- <sup>18</sup>O. Esenturk, J. S. Melinger, and E. J. Heilweil, "Terahertz mobility measurements on poly-3-hexylthiophene films: Device comparison, molecular weight, and film processing effects," *J. Appl. Phys.* **103**, 023102 (2008).
- <sup>19</sup>T. J. Magnanelli, S. Engmann, J. K. Wahlstrand, J. C. Stephenson, L. J. Richter, and E. J. Heilweil, "Polarization dependence of charge conduction in conjugated polymer films investigated with time-resolved terahertz spectroscopy," *J. Phys. Chem. C* **124**, 6993 (2020).
- <sup>20</sup>T. R. Arend, A. Wimmer, G. Schweicher, B. Chattopadhyay, Y. H. Geerts, and R. Kersting, "Band transport and trapping in didodecyl [1]benzothieno [3,2-*b*] [1]benzothiophene probed by terahertz spectroscopy," *J. Phys. Chem. Lett.* **8**, 5444 (2017).
- <sup>21</sup>D. Tsokkou, P. Cavassin, G. Rebetez, and N. Banerji, "Bipolarons rule the short-range terahertz conductivity in electrochemically doped P3HT," *Mater. Horiz.* **9**, 482 (2022).
- <sup>22</sup>L. Shaw, P. Hayoz, Y. Diao, J. A. Reinspach, J. W. F. To, M. F. Toney, R. T. Weitz, and Z. Bao, "Direct uniaxial alignment of a donor-acceptor semiconducting polymer using single-step solution shearing," *ACS Appl. Mater. Interfaces* **8**, 9285 (2016).
- <sup>23</sup>R. E. Glover and M. Tinkham, "Conductivity of superconducting films for photon energies between 0.3 and 40kT<sub>g</sub>," *Phys. Rev.* **108**, 243 (1957).
- <sup>24</sup>S. Funk, G. Acuna, M. Handloser, and R. Kersting, "Probing the momentum relaxation time of charge carriers in ultrathin layers with terahertz radiation," *Opt. Express* **17**, 17450 (2009).
- <sup>25</sup>D. Khim, A. Luzio, G. E. Bonacchini, G. Pace, M.-J. Lee, Y.-Y. Noh, and M. Caironi, "Uniaxial alignment of conjugated polymer films for high-performance organic field-effect transistors," *Adv. Mater.* **30**, 1705463 (2018).
- <sup>26</sup>J. Lenz, M. Statz, K. Watanabe, T. Taniguchi, F. Ortman, and R. T. Weitz, "Charge transport in single polymer fiber transistors in the sub-100 nm regime: Temperature dependence and Coulomb blockade," *J. Phys. Mater.* **6**, 015001 (2023).
- <sup>27</sup>N. F. Mott and E. A. Davis, *Electronic Processes in Non-Crystalline Materials* (Clarendon Press, 1979).
- <sup>28</sup>N. F. Mott and M. Kaveh, "Metal-insulator transitions in non-crystalline systems," *Adv. Phys.* **34**, 329 (1985).
- <sup>29</sup>D. Sailer, A. Bornschlegl, and R. Kersting, "Screening within accumulation layers of molecular semiconductors," *Appl. Phys. Lett.* **117**, 083301 (2020).
- <sup>30</sup>V. Podzorov, E. Menard, A. Borissov, V. Kiryukhin, J. A. Rogers, and M. E. Gershenson, "Intrinsic charge transport on the surface of organic semiconductors," *Phys. Rev. Lett.* **93**, 86602 (2004).
- <sup>31</sup>T. Lindner, G. Paasch, and S. Scheinert, "Hysteresis in organic field-effect devices: Simulated effects due to trap recharging," *J. Appl. Phys.* **98**, 114505 (2005).